Nonlinear Response of Nanostructured Graphene to Circularly Polarized Light

François Aguillon, Andrei Borisov

Nonlinear Response of Nanostructured Graphene to Circularly Polarized Light.

François Aguillon*,† and Andrei G. Borisov*,†,‡

†*Institut des Sciences Moléculaires d'Orsay (ISMO), UMR 8214, CNRS, Université Paris-Saclay, 91405 Orsay Cedex, France.*

‡*DIPC, Paseo Manuel de Lardizabal 5, Donostia - San Sebastián 20018, Spain*

E-mail: francois.aguillon@universite-paris-saclay.fr; andrei.borissov@universite-paris-saclay.fr

Phone: +33 (0)1 69157697

Abstract

Using the tight-binding description of graphene and the time dependent density matrix approach we theoretically address the nonlinear response of plasmonic graphene nanostructures to the circularly polarized light. The intensity and polarization of emitted harmonics depend on the symmetry of the system and can be analyzed applying the Neumann's principle. We find that for the nanoflakes comprising thousands of carbon atoms this is the symmetry of the carbon atom arrangement on atomic scale that determines the nonlinear response. Therefore it might be very different from the nonlinear response predicted using the macroscopic geometry. For the compound systems made of several nanoflakes we reveal the role of the near field interactions in intensity and circular polarization states of emitted harmonics. Finally we show that symmetry break by e.g. lattice defects strongly affects the nonlinear response of graphene nanoflakes to the circularly polarized light. Our work extends theoretical studies of the nonlinear optical properties of graphene nanomaterials towards spin carrying light beams.

Introduction

Controlling the nonlinear light-matter interaction at the nanoscale allows one to probe and to manipulate electronic excitations and opens up numerous perspectives in spectroscopy reaching atomic scale spatial resolution,[1–3] as well as in design of the on-chip devices for the ultrafast electronics,[4–7] for the characterization of the optical pulses,[8,9] and for the nonlinear integrated photonic circuits.[10–12] This list can be further extended citing such applications as nonlinear metrology[13] and nonlinear sensing,[14,15] among others. In this respect, the resonance between the incident electromagnetic radiation and collective electron excitations in metals and 2D materials, plasmons, allows for the strong near field enhancement,[16–19] provokes ultrafast electron dynamics[20–23] and increases the nonlinear response.

Numerous studies of the frequency conversion at plasmon resonance performed so far mainly reported results obtained for the linearly polarized incident light.[15,21,24–29] At the same time, recent interest in utilizing nonlinear metasurfaces for manipulating the structured light[30–42] requires theoretical analysis of the nonlinear optical processes triggered in plasmonic nanoparticles by the spin and orbital momentum carrying light beams. Such an analysis has been recently performed using quantum or hydrodynamic approaches for metal nanoparticles.[43–45] Along with metals, 2D materials offer unprecedented opportunities in various fields of nanotechnology[46,47] including nanoscale chiral valley-photon interfaces.[48–50] In particular, graphene features electrically tunable plasmon resonances in the linear response,[51–54] as well as strong and tunable nonlinear response.[15,29,55–65] This latter is under the focus of the present study.

Here, using a time-dependent density matrix approach and tight-binding description of graphene (TDDM-TB) we study generation of the circularly polarized harmonics from graphene nanostructures excited by the circularly polarized fundamental wave at resonance with dipolar plasmon of the nanoparticle. The circular polarization states of harmonic generation are governed in this case by selection rules imposed by the symmetry of the system which might vary depending on the level of resolution. Thus, for the bulk crystals, infi-

nite 2D materials, and for the molecules selection rules are determined by the symmetry at microscopic level, i.e. the symmetry of atomic lattice,[66–68] or the symmetry of atomic arrangement within the molecule.[69,70] However, recent experiments performed with plasmonic gold metamaterials revealed that selection rules for circular polarization in the nonlinear optical response might be determined by the macroscopic rotational symmetry.[39–41]

In this work we address the respective role of the macro- and micro- symmetries in the circular polarization of frequency harmonics relevant to explain the experiments. The quantum-mechanical studies of electron dynamics in plasmonic nanoobjects with experimental dimensions are impossible even using the simplified tight-binding description. Nonetheless, the TDDM-TB approach allows one to consider graphene nanoflakes comprising thousands of carbon atoms. In this situation the plasmon modes are well developed as we further discuss in Supporting Information (SI). Moreover, one can meaningfully consider the difference between the macroscopic symmetry set by the macroscopic geometry of the nanoflake and the microscopic symmetry at atomic level set by the honeycomb lattice enclosed by the macroscopic geometrical form. With examples of the point defects at very low concentration, and misalignment of the one of the nanoflakes in the compound system, we also study the effect of the microscopic symmetry break as well as possible symmetry retrieval owing to statistical average over the imperfections in large systems.

The paper is organized as follows. First, we briefly describe the method and discuss the results obtained for ideal and defective individual graphene nanoflakes of various geometries. In the second part of the paper, we show the TDDM-TB results obtained for an ideal and defective compound system made of several nanoflakes. Conclusions of this work and outlook are presented at the end of the paper.

Unless otherwise stated atomic units are used.

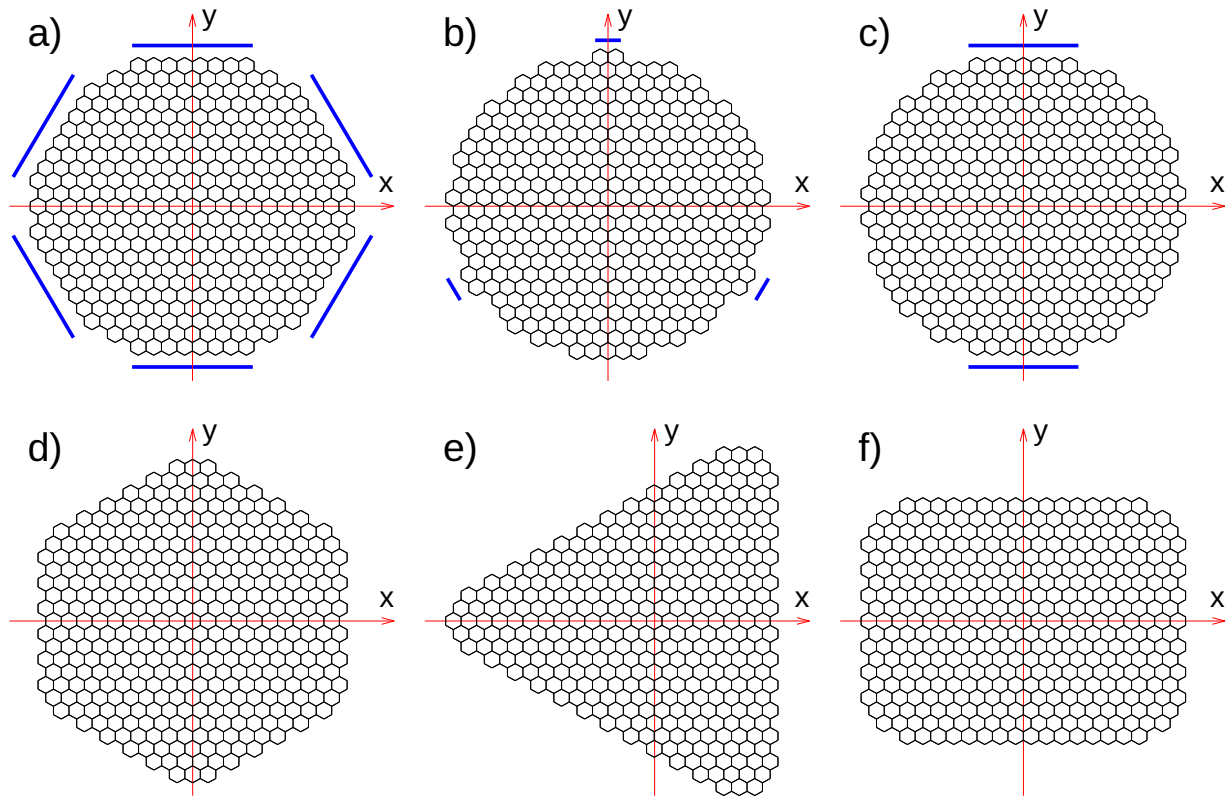

Figure 1: Sketch of the nanoflakes studied in the present work. At the macroscopic scale, the nanoflake is defined by its global shape. Panels a-c: circle, panel d: hexagon, panel e: triangle, panel f: rectangle. At the microscopic scale the symmetry of the nanoflake is set by the orientation and by the centering of the honeycomb lattice with respect to the global geometry. In panels a,d,e,f the geometrical center of the structure is in hollow location of graphene lattice, panel b – on top location, panel c – bridge location. Blue lines in panels a–c help in finding the identical zigzag sections at the edges of the disc (this sets the rotational symmetry of the system at atomic level). See also Table 1. Please note that for sake of visibility, the size of the nanoflakes shown here ($N_C \sim 800$ carbon atoms) is much smaller than the actual one used in calculations ($N_C \sim 10^4$ carbon atoms).

Individual graphene nanoflakes

Geometry

In order to access the role of the symmetry in nonlinear response of graphene nanostructures to the circularly polarized fundamental wave we have chosen several representative model examples illustrated in Fig. 1. These nanoflakes encompass broad spectrum of the combinations between the symmetry defined by macroscopic geometry and atomic-scale symmetry

defined by the arrangement of the carbon atoms within geometrical borders. It is worth noting that in Fig. 1 and below we use the coordinate system where the z-axis is perpendicular to graphene plane and y- and x- axes are in-plane.

The nanoflakes ($\mathcal{F}$) with circular macroscopic geometry (Fig. 1a,b,c) are obtained by cutting a circle of the radius $R = 200$ a_0 (the Bohr radius $a_0 \approx 0.53$ Å) from an ideal graphene plane. The carbon atoms with single neighbor are removed at the borders. The relaxation of graphene lattice because of the finite size is neglected. We address this issue in more details in SI. Placing the center of the circle at the hollow site (Fig. 1a) we obtain the graphene nanoflake $\mathcal{F}_6^\infty$. Here, the superscript ∞ stands for the rotational symmetry of the macroscopic circular object with respect to the z- axis while the subscript 6 stands for the microscopic rotational symmetry given by the grid of carbon atoms forming the nanoflake (C6, with respect to the z- axis). Similarly, placing the center of the circle at the top site (Fig. 1b) we obtain the graphene nanoflake $\mathcal{F}_3^\infty$, and placing the center of the circle at the hollow site (Fig. 1c) we obtain the graphene nanoflake $\mathcal{F}_2^\infty$.

Along with nanoflakes described above and characterized by the difference in their macroscopic and microscopic rotational symmetries, we have also considered the the hexagonal $\mathcal{F}_6^6$ (Fig. 1d), equilateral triangle $\mathcal{F}_3^3$ (Fig. 1e), and rectangular $\mathcal{F}_2^2$ (Fig. 1f) nanoflakes. Here, the macroscopic rotational symmetry is the same as the microscopic rotational symmetry. We set the geometry of the hexagonal and triangular structures such that edges are armchair leading to slower plasmon decay into the electron hole pairs via the edge scattering (Landau damping)[71–76] and thus to better defined plasmon modes.

The nanoflakes of N_C carbon atoms are electrostatically doped by n_{dop} electrons in such a way that their dipolar plasmon resonance frequencies ω_{DP} determined from the linear response are most of the time in the range of 0.2–0.3 eV. Table 1 summarizes the properties of the individual graphene nanoflakes sketched in Fig. 1 and studied here.

Table 1: Characteristics of graphene nanoflakes sketched in panels a–f of Fig. 1. For the details see the text of the paper.

Panel	Shape	Centering	Symmetry	N_C	n_{dop}	$\omega_{\rm DP}$(eV)
a	Disc	hollow	$\mathcal{F}_6^\infty$	13452	60	0.235
b	Disc	top	$\mathcal{F}_3^\infty$	13441	60	0.245
c	Disc	bridge	$\mathcal{F}_2^\infty$	13432	60	0.242
d	Hexagon	hollow	$\mathcal{F}_6^6$	13284	60	0.320
e	Triangle	hollow	$\mathcal{F}_3^3$	13548	60	0.263
f	Rectangle	hollow	$\mathcal{F}_2^2$	13424	60	0.275

Calculation of electron dynamics

The linear and nonlinear response of graphene nanoflakes is studied using the calculations of their electron dynamics driven by an external electromagnetic field. Our explicitly time-dependent approach, TDDM-TB, has been presented in great detail elsewhere[77] (see also Refs.[78,79]). It builds on the tight-binding description of electron dynamics in π-bands of graphene that allows one to describe the ultra-fast nonlinear response of large graphene nanostructures, or pristine graphene.[15,80–83] Essentially, present TDDM-TB is a further development of the theoretical method proposed earlier to address linear and nonlinear effects in graphene plasmonics.[71,84] We only outline here the aspects specific for the present study, where the quantum master equation for the time-evolution of the density matrix $\hat{\rho}$[85–88]

$$i\frac{\partial\hat{\rho}}{\partial t} = \left[\hat{H},\hat{\rho}\right] - i\gamma\left(\hat{\rho}-\hat{\rho}^{(0)}\right), \tag{1}$$

is solved using the split-operator time-propagation.[89] The tight-binding hamiltonian of the system $\hat{H}$ comprises the hamiltonian of the ground-state system, dynamical interaction between the charges induced at carbon atom lattice sites, and an external potential owing to the incident electromagnetic radiation. The nonretarded approximation is used because the considered systems are small on the scale given by the electromagnetic wavelength. The second term on the right-hand-side of the equation is the simplified form of the Lindblad super-operator and it describes the relaxation to the ground-state density matrix $\hat{\rho}^{(0)}$ with a

rate γ. Here we use $\gamma = 15$ meV to represent the plasmon decay by excitation of the optical phonons in graphene.[51,90–92]

The polarisation states and intensity of the emitted harmonics are obtained from the analysis of the time-dependent dipole $\mathbf{p}(t)$ induced in graphene nanoflakes by an incident electromagnetic pulse propagating in positive direction of z-axis. We use the left-handed (as seen from the receiver) circularly polarized Gaussian pulse with spin angular momentum SAM= +1. An electric field vector of the fundamental pulse $\mathbf{E}(t)$ is rotating anticlockwise in the plane of graphene nanostructure:

$$\mathbf{E}(t) = E_0 \ \exp\left[-\left(\frac{t-t_0}{\tau}\right)^2\right] \ [\hat{e}_x \cos(\omega_0 t) + \hat{e}_y \sin(\omega_0 t)] \tag{2}$$

where $\hat{e}_x$ ($\hat{e}_y$) is the unit length vector in positive x- (y-) direction. The FWHM duration of the pulse equals to five optical periods $\tau = \frac{5\pi}{\omega\sqrt{\ln 2}}$ resulting in the spectral width $\triangle\omega \approx$ 30 meV within the considered range of ω_0. The time of arrival is set as $t_0 = 3.4\ \tau$, and the field amplitude $E_0 = 2 \times 10^{-5}$ a.u. (≈ 10 mV/nm) has been used. The fundamental wave is at resonance with dipolar plasmon of graphene nanoflake $\omega_0 = \omega_{\mathrm{DP}}$ which allows to maximise the nonlinear response.[29,55,59,93]

The frequency resolved x- and y-components of the induced dipole $\mathbf{p}(\omega)$ are obtained from the time-to frequency Fourier transform

$$p_\zeta(\omega) = \hat{e}_\zeta \cdot \mathbf{p}(\omega) = \frac{1}{\sqrt{2\pi}} \int_{-\infty}^{+\infty} \hat{e}_\zeta \cdot \mathbf{p}(t) \ e^{i\omega t} \ dt, \qquad \zeta = (x, y). \tag{3}$$

In particular, $p_x(h\omega_0)$ and $p_y(h\omega_0)$ characterise the nonlinear dipole induced at harmonic frequencies $h\omega_0$, where an integer h stands for harmonic order. To analyse the polarisation, it is useful to introduce the rotating vectors $\hat{e}_\pm = \frac{1}{\sqrt{2}} (\hat{e}_x \pm i \ \hat{e}_y)$ with SAM= ± 1 (the $e^{-i\omega t}$ time dependence of the Fourier components is assumed). The induced dipole $\mathbf{p}(\omega) = p_x(\omega) \ \hat{e}_x +$

$p_y(\omega)\ \hat{e}_y$ can be represented in the rotating vector basis as

$$\mathbf{p}(\omega) = p_+(\omega)\ \hat{e}_+ + p_-(\omega)\ \hat{e}_-,$$
$$p_\pm(\omega) = \frac{1}{\sqrt{2}}\left[p_x(\omega) \mp i p_y(\omega)\right]. \tag{4}$$

The dipole projections on rotating basis vectors are used to analyse the polarization of the frequency harmonics. The latter is characterized by the polarisation index $\mathcal{I}_p(h\omega_0)$ defined as follows

$$\mathcal{I}_p(h\omega_0) = \frac{|p_+(h\omega_0)| - |p_-(h\omega_0)|}{|p_+(h\omega_0)| + |p_-(h\omega_0)|} \tag{5}$$

The $\mathcal{I}_p(h\omega_0)$ gives the ratio of the minor and major axes of the ellipse traced in the (x, y)-plane by the nonlinear dipole generated at harmonic h. It is positive (negative) for the general left- (right-) handed elliptical polarization ($\mathcal{I}_p = \pm 1$ for the circular polarization, and $\mathcal{I}_p = 0$ for the linear polarization).

Nonlinear response to circularly polarized fundamental wave

We start our discussion of the nonlinear response of graphene nanostructures to the circularly polarized light and of the role of the symmetry in the polarization states of emitted harmonics with an example of individual graphene nanoflakes sketched in Fig. 1 and characterized in Table 1. Since the intensity and polarization of the emitted harmonics is given by the absolute value and polarization of the nonlinear dipole moment induced in the nanostructure we focus our analysis on the latter. In Fig. 2 we show the frequency dependence of the absolute values of the projections $|p_\pm(\omega)|$ of the induced dipole on the rotating basis vectors. The fundamental circularly polarized Gaussian pulse with SAM= +1 is resonant with dipolar plasmon of the nanoflakes $\omega_0 = \omega_{\rm DP}$. The peaks in $|p_\pm(\omega)|$ correspond to the dipole induced at harmonics of the fundamental frequency $\omega = h\omega_0$. As we show in SI, present characteristics of the fundamental pulse allow one to describe the nonlinear response of the nanostructure using the first order of the perturbation theory. In particular, the variation of the amplitude

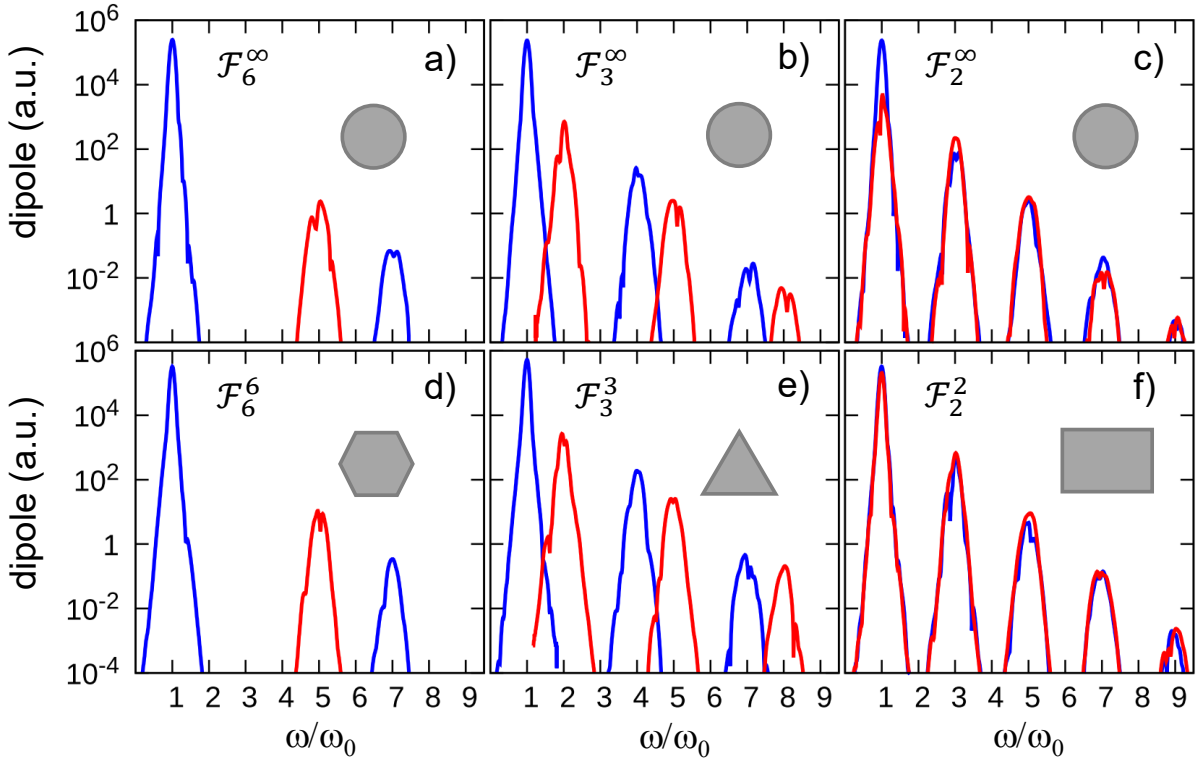

Figure 2: Spectral analysis of the nonlinear dipole induced in graphene nanoflakes characterized in Fig. 1 and in Table 1. The fundamental electromagnetic field is given by the circularly polarized Gaussian pulse with SAM= +1 and frequency ω_0 resonant with dipolar plasmon of the nanoflake $\omega_0 = \omega_{\rm DP}$. The inserts sketch the macroscopic geometry, and give the microscopic symmetry of the nanoflakes. In blue (red) we show the frequency dependence of the absolute value of the projections $|p_+(\omega)|$ ($|p_-(\omega)|$) of the induced dipole on rotating basis vectors with SAM= +1 (SAM= −1). The frequency is measured in units of ω_0. The peaks at $\omega = h\omega_0$ correspond to the generation of the frequency harmonics.

of the induced dipole at harmonic frequencies can be found from $p_\pm(h\omega_0) = \alpha_\pm^{(h)} E_0^h$, where $\alpha_\pm^{(h)}$ is the hyperpolarizability. The final width of the harmonic peaks reflects in the present case primarily the finite duration of the fundamental Gaussian pulse.

It is clear from the TDDM-TB results that the nonlinear dipole is excited only at certain harmonic frequencies, and in many situations only one projection $p_+(\omega)$ or $p_-(\omega)$ is present so that the induced dipole and thus the emitted harmonic is circularly polarized with SAM= +1 (SAM= −1). However, for some harmonics (Fig. 2c and Fig. 2f) both projections $p_+(\omega)$ and $p_-(\omega)$ are present at $h\omega_0$. This indicates an elliptic polarization of emitted harmonics (in a specific situation when $|p_+| = |p_-|$ the corresponding harmonics are linearly polarized).

The TDDM-TB results can be understood using the selection rules for the circular polarization states of harmonic generation which can be obtained from the Neumann's principle for tensors.[94,95] For the circularly polarized fundamental wave the selection rules are[38–41,67,68]

$$h = \mathcal{S}\ j \pm 1, \qquad h \geq 0, \tag{6}$$

where j and h are integers (h defines the harmonic order), $\mathcal{S}$ is the order of the rotation symmetry with respect to the z-axis, and ± 1 defines the circular polarization of the induced nonlinear dipole at $h\omega_0$ harmonic frequency. For the "$+$" ("$-$") sign the induced nonlinear dipole and the electric field vector of the fundamental wave are co- (counter-) rotating in the plane of graphene nanostructure. Correspondingly, the harmonic field propagating in positive direction of z-axis has the same or an opposite circular polarization state (or handiness) as compared to that of the fundamental wave. For the left-handed fundamental wave with SAM=+1, the left- (SAM= +1) or right- (SAM= -1) handed harmonics are shown with blue (red) color in Fig. 2. It is worth noting that as we discuss in Supporting Information (SI), the above selection rules can be generalised to any moment of the charge density induced at harmonic frequency within the nanoflake.

Considering the fundamental field with SAM=+1, Table 2 provides the polarization (SAM) and order (h) of the frequency harmonics allowed by selection rules in Eq. 6 for the symmetries relevant for the discussion of the nonlinear response shown in Fig. 2 and calculated with TDDM-TB for individual graphene nanoflakes sketched in Fig. 1. Notice that for the C2 rotational symmetry the odd harmonics are generated in both polarization states, and even harmonics are forbidden. Moreover, for the circular geometry with an infinite rotation symmetry only $j = 0$ and $h = 1$ is possible, i.e. one expects no dipolar polarization at $h > 1$ harmonic frequencies.

The frequency analysis of the induced dipole in Fig. 2 demonstrates that the TDDM-TB results are in full accord with above selection rules when these are derived using microscopic

Table 2: Polarization (SAM) and order (h) of the frequency harmonics allowed by selection rules given by Eq. 6, in the case of the rotational symmetries relevant for the present study. The fundamental field is circularly polarized with SAM= +1. Integer $j \geq 0$.

symmetry	$\mathcal{S}$	SAM= +1	SAM= −1
C1	1	$h = j$ $h = 0, 1, 2, ...$	$h = j$ $h = 0, 1, 2, ...$
C2	2	$h = 1 + 2j$ $h = 1, 3, 5, ...$	$h = 1 + 2j$ $h = 1, 3, 5, ...$
C3	3	$h = 1 + 3j$ $h = 1, 4, 7, ...$	$h = 2 + 3j$ $h = 2, 5, 8, ...$
C6	6	$h = 1 + 6j$ $h = 1, 7, 13, ...$	$h = 5 + 6j$ $h = 5, 11, 17, ...$
C∞	∞	$h = 1$	not possible

symmetry given by the arrangement of carbon atoms within the macroscopic geometrical for of the nanoflake. It is spectacular that

- For the given microscopic symmetry order $\mathcal{S} = 2, 3, 6$, the induced dipole is at the same harmonics and with the same handiness for the $\mathcal{F}_{\mathcal{S}}^{\infty}$ and $\mathcal{F}_{\mathcal{S}}^{\mathcal{S}}$ nanoflakes with absolutely different (∞ or $\mathcal{S}$) macroscopic symmetries;

- The efficiency of the frequency conversion determined by the amplitude of the induced dipole is similar for the nanoflakes with the same microscopic symmetry albeit their macroscopic symmetry might be different.

It thus follows from the TDDM-TB results above, that for ideal graphene nanoflakes comprising $N_C \sim 13500$ carbon atoms the polarization states of the frequency harmonics are determined by the microscopic atomic-scale symmetry of the nanostructure. Considering experimental situation, the question then naturally arises about an effect of possible perturbation of this symmetry e.g. by the defects, adsorbates, or by graphene lattice relaxation

in presence of constraints imposed by the substrate.[96] In order to assess the sensitivity of the selection rules to the perturbation of atomic scale symmetry we have performed the TDDM-TB calculations for graphene nanoflakes with point defects.

Role of the point defects

We modelled point defects by removing carbon atoms at randomly chosen lattice sites of graphene nanostructures. Despite its simplicity, this commonly used approximation[97–101] yields the nonlinear response in semi-quantitative agreement with more involved modeling of the realistic defects in graphene such as $V_1(5-9)$ fully relaxed monovacancy defects[102–104] (see recent work[77] for the linearly polarized fundamental wave, and present SI for the circularly polarized fundamental wave).

In Fig. 3 we show the effect of the carbon atom vacancies using representative results obtained for the nonlinear response of triangular graphene nanoflake with armchair boundary excited by the fundamental circularly polarised (SAM= +1) gaussian pulse resonant with dipolar plasmon of the nanostructure. An ideal (defect-free) $\mathcal{F}_3^3$ nanoflake comprises $N_C = 10194$ carbon atoms, and it is electrostatically doped with $n_{dop} = 20$ electrons resulting in dipolar plasmon frequency $\omega_{\rm DP} = 0.236$ eV.

Comparison between an ideal and defective nanostructure in Fig. 3a reveals that the presence of a single (!) atom vacancy defect strongly affects the nonlinear response. From the spectral analysis of the projections $p_\pm(\omega)$ of the induced dipole on rotating basis vectors with SAM= ± 1 it follows that the selection rules for the circular polarization states of harmonic generation are determined by the C1 symmetry and not by the C3 symmetry of an ideal $\mathcal{F}_3^3$ nanoflake (see Table 2). This is consistent with loss of the microscopic C3 symmetry of the carbon atom arrangement within an ideal nanostructure since the defective nanostructure is not symmetric on the atomic scale (C1 symmetry). For the defective nanostructure the dipolar polarization with projections on both SAM= +1 and SAM= −1 rotating basis vectors appears at all harmonic orders h (see bottom sub-panel in Fig. 3a). The emitted

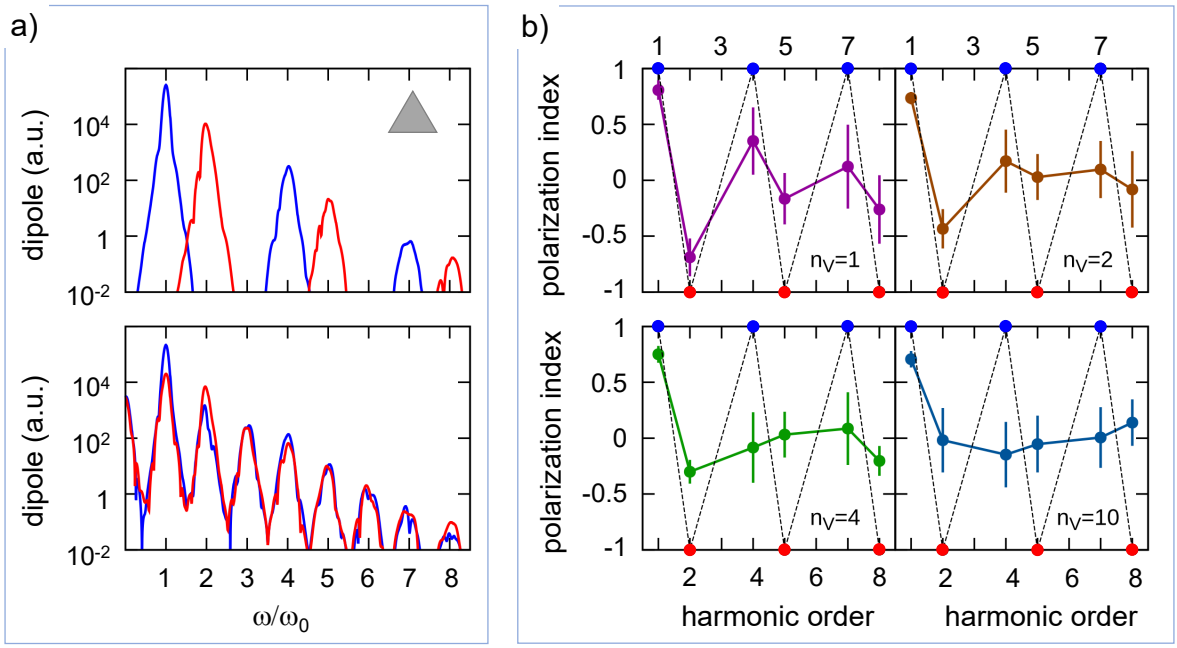

Figure 3: An effect of the carbon atom vacancies on the nonlinear response of the triangular graphene nanoflake with armchair boundary. In the defect-free case the $\mathcal{F}_3^3$ nanoflake comprizes $N_C = 10194$ carbon atoms, and it is electrostatically doped whith $n_{dop} = 20$ electrons. The fundamental circularly polarised (SAM= +1) gaussian pulse is resonant with dipolar plasmon of the nanostructure $\omega_0 = 0.236$ eV. Group of panels a): Spectral analysis of the nonlinear dipole for an ideal nanoflake (top sub-panel) and nanoflake with single randomly positioned carbon atom vacancy (bottom sub-panel). In blue (red) we show the frequency dependence of the absolute value of the projections $|p_+(\omega)|$ ($|p_-(\omega)|$) of the induced dipole on rotating basis vectors with SAM= +1 (SAM= −1). The frequency is measured in units of ω_0. The peaks at $\omega = h\omega_0$ correspond to the generation of the frequency harmonics. Group of panels b): Solid lines with dots show dependence of the polarisation index $\mathcal{I}_p(h\omega_0)$ (see Eq. 5) on harmonic order h for the frequency harmonics present in a defect-free case. Different panels correspond to the results obtained with different number n_V of the randomly distributed carbon atom vacancies indicated in the insert of each panel. For each n_V value, $\mathcal{I}_p(h\omega_0)$ is obtained as an average over five random samples, and the vertical error bars display the standard deviation. Blue (red) dots at $\mathcal{I}_p = \pm 1$ connected by dashed lines illustrate selection rules for the SAM= +1 (SAM= −1) polarization states for the defect-free $\mathcal{F}_3^3$ nanoflake (see the spectral analysis on the top of panel a).

harmonics are thus characterized by an elliptical polarization. It is worth noting that since bottom sub-panel of Fig. 3a mainly serves to underline qualitative difference with an ideal nanostructure, no statistical averaging over vacancy positions has been performed here.

This statistical analysis has been performed for the characterization of the vacancy dependence of the polarisation index $\mathcal{I}_p(h\omega_0)$ at different harmonic frequencies as reported in

group of panels in Fig. 3b. Focusing on the possible interest of the nanostructure for the generation of the circularly polarized beams at certain harmonics with no emission at other harmonics, we only show here results for the harmonic orders h present in a defect-free case. Obviously, it follows from Fig. 3a that defects trigger generation of all frequency harmonics. We seek then whether at least the polarisation of the harmonics present for an ideal nanostructure will remain for the defective nanoflake.

Each sub-panel of Fig. 3b corresponds to the situation where n_V carbon atom vacancies are randomly distributed within graphene lattice (n_V is indicated at the bottom right of each sub-panel). For each n_V value, the polarization index $\mathcal{I}_p(h\omega_0)$ given by Eq. (5) is obtained as an average over five random samples. The vertical error bars display the standard deviation of the results. Results shown in Fig. 3b fully confirm the trends observed in Fig. 3a. In particular, for the defective structure the frequency harmonics are characterized by an elliptical polarization with generally low polarization index and arbitrary handiness. The circular polarization and the handiness of the frequency harmonics of an ideal nanostructure is generally lost. The higher is harmonic order h the stronger it is affected by the defects already at their low concentration. We find that it is only the circular polarization and handiness of the second harmonic predicted by the selection rules for an ideal structure that persists at low defect concentration, even though it disappears already for 10 missing-atom defects randomly distributed within the structure (0.1 % of defect concentration).

It is worthy to note that along with circular polarization lattice defects strongly affect the intensity of harmonics emitted by graphene nanoflake as follows from results in Fig. 4. In this figure, we show an absolute value of the induced dipole $p(h\omega_0) = \sqrt{|p_+(h\omega_0)|^2 + |p_-(h\omega_0)|^2}$ calculated for different number of vacancy defects at fundamental and harmonic frequencies $h = 1, ..., 8$. For the frequency harmonics allowed by the selection rules for an ideal triangular C3 nanoflake (see Table 2), even a small number of vacancy defects appreciably reduces not only the polarization index as shown in Fig. 3b, but also the induced nonlinear dipole and therefore the intensity of emitted harmonics. Thus we obtain about 6 times reduction of the

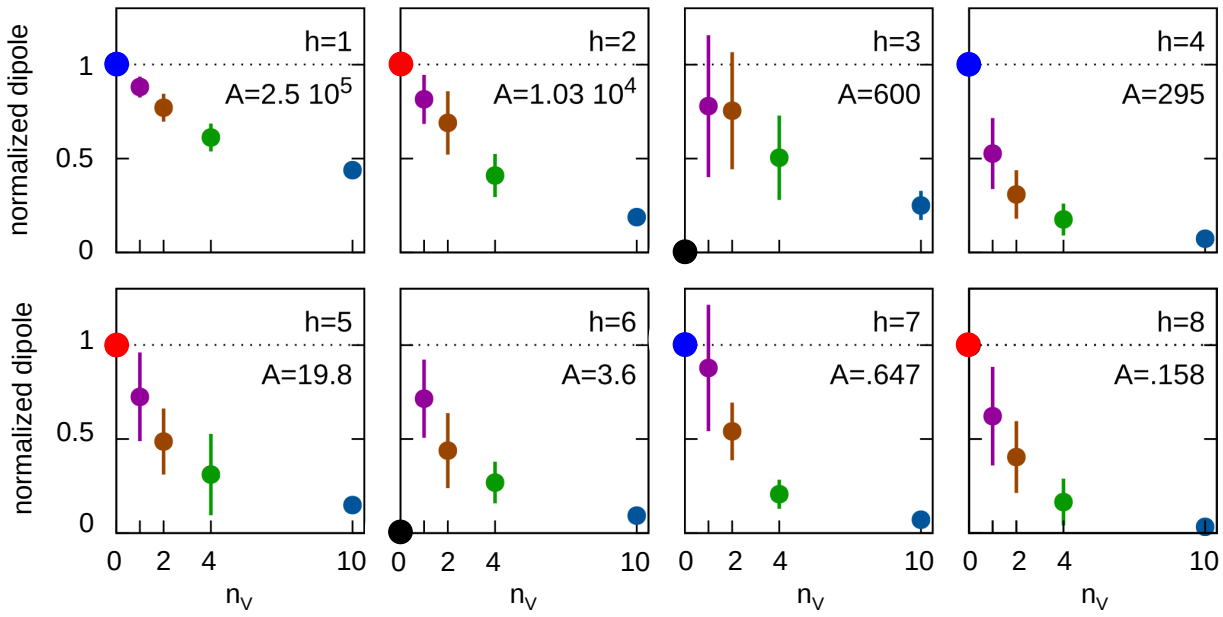

Figure 4: An effect of the carbon atom vacancies on the nonlinear response of the triangular graphene nanoflake in the same conditions as in Fig. 3. An absolute value of the normalized dipole induced at harmonic frequencies $p(h\omega_0) \times A^{-1}$ is shown as function of the number of vacancy defects n_V. For each n_V value, $p(h\omega_0)$ is obtained as an average over five random samples, and the vertical error bars display the standard deviation of the results. Panels of the figure correspond to the results obtained for different harmonic orders h given at the top right of each panel together with normalization factor A given in atomic units. For further details see the text and caption of Fig. 3.

second harmonic intensity and about 16 times reduction of the forth harmonic intensity for the $n_V = 10$ vacancy defects present in the nanoflake comprising $N_C = 10194$ carbon atoms in an ideal lattice. The harmonic orders $h = 3, 6$ forbidden by the symmetry selection rules for an ideal nanoflake are generated due to the presence of the defects. Their intensity then first rises from zero as soon as a single defect appears within the nanostructure, but then it promptly decreases for more defects.

Results similar to those reported in Fig. 3 and in Fig. 4 are obtained for all graphene nanostructures considered in this work. The effect of the carbon atom vacancies on the nonlinear response to the circularly polarized light calculated here is inline with our previous studies of nonlinear response of graphene nanoflakes for the linearly polarised fundamental wave.[77,105,106] It can be related to the defect-induced inelastic scattering and dephasing of

the optically excited electrons that (i) breaks the symmetry constraints behind the electron dynamics, (ii) leads to the quenching of the plasmon modes and associated near field enhancement. In turn, (i) and (ii) affect the selection rules for harmonic generation and reduce the nonlinear response. In this respect, as we show in SI, the inner-vacancies are more efficient perturbers than the edge-vacancies, and even than the extended edge defects obtained by removal of one zigzag section of the circular $\mathcal{F}_6^\infty$ graphene nanoflake. We tentatively attribute this result to an inner-vacancy acting as an efficient electron scattering center added to the system by "cutting" CC connections transporting electron flux in hexagonal electric network, while an edge-vacancy only modifies the boundary conditions for the edge scattering.

Compound plasmonic system

An arrangement of identical graphene nanoflakes of certain symmetry in a compound system of different symmetry represents an interesting situation where for the noninteracting entities the selection rules for the circularly polarized harmonic generation will be that of the individual nanoflakes, while the interaction between nanoflakes is responsible for the change of the selection rules. Above we have demonstrated an extreme sensitivity of the circularly polarised harmonic generation to atomic-scale defects. Roughly speaking, one can say that the behaviour is binary. For an ideal symmetry of atomic arrangement within the nanoflake the nonlinear response is determined by this symmetry, and as soon as tiny fraction of the defects appear, the C1 symmetry drives the nonlinear response of the system. For the compound system we now want to demonstrate situations where the evolution of selection rules is progressive.

Specifically, in Fig. 5 we analyse the nonlinear response of the compound nanostructure created by arranging three identical circular $\mathcal{F}_6^\infty$ nanoflakes comprising $N_C = 13542$ carbon atoms (the radius of the nanoflake ≈ 10 nm) in the equilateral triangle with separation D

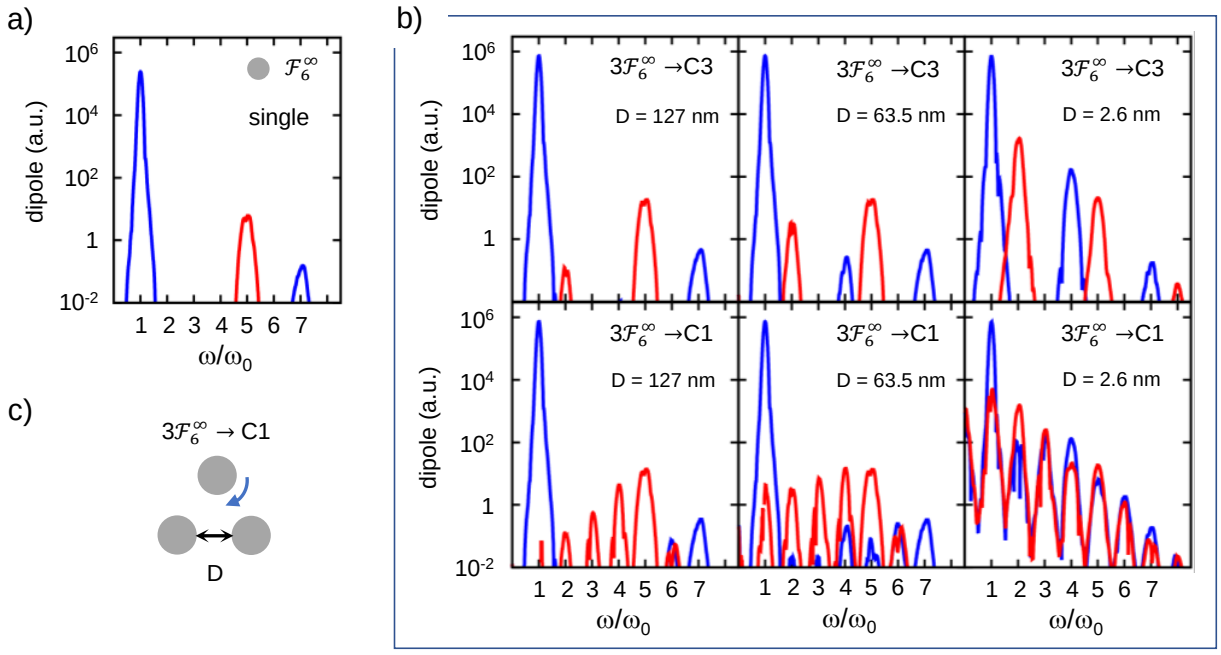

Figure 5: The nonlinear response of the $3\mathcal{F}_6^\infty$ compound structure formed by identical hollow-centered circular $\mathcal{F}_6^\infty$ graphene nanoflakes arranged in equilateral triangle. The nanoflakes comprise $N_C = 13542$ carbon atoms and are electrostatically doped with $n_{dop} = 50$ electrons resulting in $\omega_{\rm DP} = 0.223$ eV. The fundamental circularly polarised (SAM= +1) gaussian pulse is resonant with dipolar plasmon of the nanostructure $\omega_0 = \omega_{\rm DP}$. Panel a: spectral analysis of the nonlinear dipole induced in an individual $\mathcal{F}_6^\infty$ graphene nanoflake used as a reference. Panel b: spectral analysis of the nonlinear dipole induced in the $3\mathcal{F}_6^\infty$ compound structure. In blue (red) we show the frequency dependence of the absolute value of the projections $|p_+(\omega)|$ ($|p_-(\omega)|$) of the induced dipole on rotating basis vectors with SAM= +1 (SAM= −1). The frequency is measured in units of ω_0. The peaks at $\omega = h\omega_0$ correspond to the generation of the frequency harmonics. Top row of sub-panels in panel b: the evolution of the nonlinear response of the compound structure with C3 symmetry of the atomic arrangement upon decreasing the separation D between the nanoflakes. Bottom row of sub-panels in panel b: the same as top row, but for the situation where one of the nanoflakes has been rotated around its centre by 15° as sketched in panel c). Rotation results in C1 microscopic symmetry of the compound structure. The inserts precise the symmetry of the compound structure, and provide the value the separation D.

between the nanoflakes. The macroscopic geometry of the system is therefore characterized by the C3 symmetry with respect to the axis perpendicular to the centre of the triangle.

First, the $\mathcal{F}_6^\infty$ nanoflakes are oriented such that the microscopic atomic-scale symmetry of the compound system is also C3, and the top row panels in Fig. 5 trace the evolution of the nonlinear response upon approaching the nanoflakes. The reference results in Fig. 5a

calculated for an individual $\mathcal{F}_6^\infty$ nanoflake, and results calculated for the $3\mathcal{F}_6^\infty \rightarrow$ C3 compound nanostructure with large separation $D = 127$ nm feature almost equivalent selection rules with three times larger dipolar polarization in the latter case. Indeed, for non interacting nanoflakes excited by the circularly polarized fundamental wave, the nonlinear response of the compound system is given by the coherent superposition of the phase-synchronized nonlinear dipoles induced in the individual $\mathcal{F}_6^\infty$ nanoflakes. The selection rules for the polarization states of the total nonlinear induced dipole can be then described by Eq. 6 for the C6 symmetry, and the total nonlinear dipole of the compound system $p_{\rm tot}(h\omega_0) = 3p(h\omega_0)$, where $p(h\omega_0)$ is the nonlinear dipole induced by the fundamental wave in each nanoflake.

Reducing separation D increases the interaction between the nanoflakes through the near fields, and the system evolves from an arrangement of individual nanoflakes of the microscopic C6 symmetry to their compound of the microscopic C3 symmetry. Additional frequency harmonics with order h and SAM predicted by the selection rules for the C3 symmetry ($h = 2$, SAM$= -1$, and $h = 4$, SAM$= +1$) progressively emerge in the spectra. For the smallest D considered here, individual nanoflakes are strongly coupled and the spectral analysis nicely reveals the circular polarization states of the C3 symmetry.

Rotation of the one of nanoflakes by a small angle $\alpha = 15^\circ$ as sketched in Fig. 5c breaks the microscopic C3 symmetry of the carbon atom arrangement which is then transformed to C1. This is while the macroscopic C3 symmetry is not changed by this transformation since the nanoflakes are of circular geometry. As follows from the TDDM-TB results for the nonlinear response shown in the bottom row of panels of Fig. 5b, reducing separation D leads to the progressive evolution of the spectra from that driven by the higher symmetry to that driven by the lower symmetry. In this respect the behaviour is similar to that obtained in the top row of panels of Fig. 5b. However there is an essential difference: for smallest D and thus for the largest near field interaction between the nanoflakes, the nonlinear dipole at all harmonic frequencies has both p_+ and p_- components as expected for the object of the C1 symmetry (see Table 2 as well as result reported in Fig. 3 for the defective $\mathcal{F}_3^3$ nanoflake).

Interestingly, as we further elaborate in SI, careful analysis of the results in Fig. 5b shows that upon rotation of one of the nanoflakes, the $h = 1, 2, 4, 5$ harmonics authorized for the *macroscopic* C3 symmetry feature nearly circular polarization in accord with corresponding selection rules (one has to consider the log scale of Fig. 5b). This holds in particular for low h, and up to the smallest $D = 2.6$ nm separation between the nanoflakes considered here. This said, the break of the microscopic C3 symmetry by rotation of one of nanoflakes leads to the overall nonlinear response grossly determined by the microscopic C1 symmetry.

Present results in light of experimental findings

We are now in a position to look for a link between present theoretical results and recent experiments studying selection rules for generation of circularly polarized harmonics from plasmonic metamaterials.[39–41] The TDDM-TB results for the single nanoflakes demonstrate that for the size of the nanoobjects addressed here the microscopic rotational symmetry of the arrangement of the carbon atoms within the system determines the circular polarization states of harmonic generation. Since an individual (plasmonic) nanostructure constitutes a building block (meta-atom) for design of metasurface or metamaterial, present theoretical result appears at odds with experimental data. Indeed, the macroscopic rotational symmetry of the metamaterial was found to explain the circular polarization states of frequency harmonics.[39–41] This is while unavoidably the defects, and an appreciable geometry deviation from an ideal will break the symmetry of the meta-atoms and of the entire metamaterial on the microscopic level reducing it to C1.

We believe that this apparent contradiction can be lifted considering an effect of the average over large number of individual nanoobjects which restores the role of the macroscopic symmetry in experimental situation. Recall that for the compound system of 3 graphene nanoflakes of C1 microscopic and C3 macroscopic symmetry (Fig. 5), the polarization states of the harmonics allowed by the C3 symmetry retain to large extent the C3 selection rules.

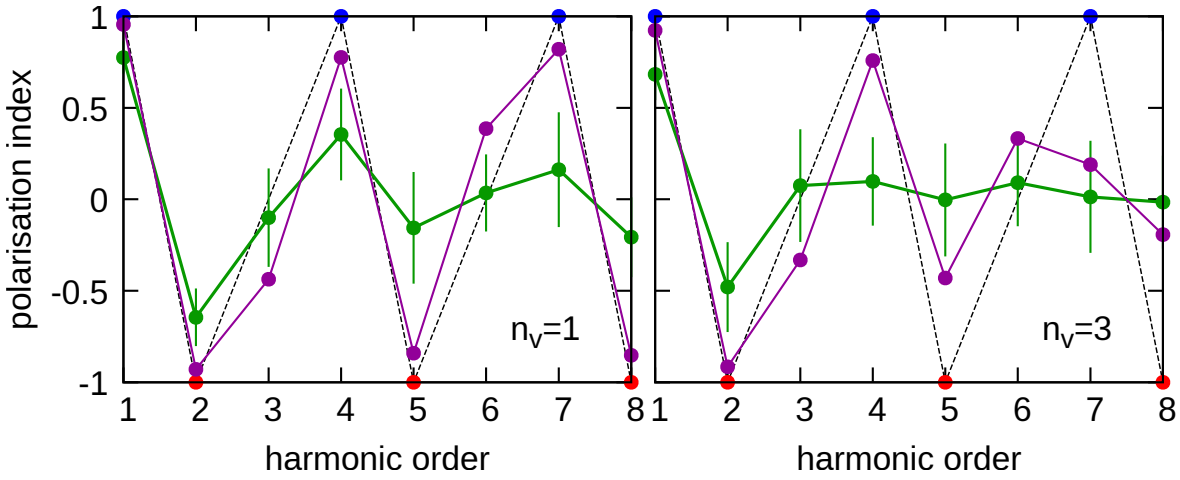

Figure 6: An effect of the carbon atom vacancies on nonlinear response of a structure comprising 50 noninteracting graphene nanoflakes. An ideal individual $\mathcal{F}_3^3$ triangular nanoflake with armchair boundary comprises $N_C = 5556$ carbon atoms and it is electrostatically doped with $n_{dop} = 10$ electrons. The fundamental circularly polarised (SAM= +1) gaussian pulse is resonant with dipolar plasmon of the nanoflake, $\omega_0 = 0.25$ eV. The nanoflakes are randomly oriented in space. For the defective structure, the n_V carbon atom vacancies are introduced at random positions within each nanoflake. We show the dependence of the polarisation index $\mathcal{I}_p(h\omega_0)$ (see Eq. 5) on harmonic order h. The left (right) panel of the figure corresponds to the situation with $n_V = 1$ ($n_V = 3$) as indicated in the inserts. Green dots connected with green line show results for an individual $\mathcal{F}_3^3$ nanoflake. Error bars correspond to the statistical average over the vacancy positions (see caption of Fig. 3b for further details). Violet dots connected with violet line show results for the structure comprising 50 nanoflakes. Blue (red) dots at $\mathcal{I}_p = \pm 1$ connected by dashed lines illustrate selection rules for the SAM= +1 (SAM= −1) polarization states for the C3 structure without defects.

Unfortunately, the TDDM-TB study of a large number of interacting nanoobjects of some 100 nm size as available experimentally is out of reach at present. However it is possible to further support our statement using model system. To this end we consider a structure made of 50 randomly positioned and randomly oriented coplanar triangular $\mathcal{F}_3^3$ graphene nanoflakes with armchair boundary. The interaction between the nanoflakes is neglected. Therefore, the total nonlinear dipole of the system is given by the vectorial sum of the nonlinear dipoles induced in individual nanoflakes by the fundamental field.

In Fig. 6 with violet dots we show the polarization index of the harmonics emitted by the structure of 50 $\mathcal{F}_3^3$ graphene nanoflakes, where $n_V = 1$ or $n_V = 3$ vacancy defects were introduced at random positions within each nanoflake. The polarization index of the

harmonics emitted by an individual defective $\mathcal{F}_3^3$ nanoflake is shown with green line, and blue (red) dots illustrate selection rules for the SAM$= +1$ (SAM$= -1$) polarization states in the case of the C3 symmetry. Obviously, for an individual nanoparticle, presence of the defects quickly degrades the polarization index of emitted harmonics inline with results shown in Fig. 3b. This is while the structure comprising several tens of the nanoflakes averages out the defect associated alternations in the nonlinear response of individual nanoparticles as far as polarization is concerned. One obtains partial retrieval of the sought circular polarization for harmonics allowed by selection rules for an ideal nanoflake, this is while all harmonic frequencies are present in nonlinear spectra in contrast with an ideal C3 symmetry. The model example above points at possibly lower sensitivity to the defects for large systems such as metasurfaces.

Conclusions and outlook

Using the TDDM-TB approach we have studied the nonlinear response of some 10^4 carbon atoms size graphene nanoflakes to the circularly polarized fundamental wave resonant with dipolar plasmon of the nanostructure. In relation with recent experiments,[39–41] particular emphasis is put on the polarization of the frequency harmonics generated by the nanostructures that can be considered as meta-atoms for nonlinear metamaterials allowing manipulation of the spin orbital momentum of light.

Three important issues are addressed in this work

1. Is it macroscopic symmetry given by the global shape of the large nanoflake or microscopic symmetry given by the arrangement of the carbon atoms within the nanostructure that determines selection rules for the circular polarization states of emitted harmonics?

2. How the polarization states of emitted harmonics are perturbed by unavoidable imperfections?

3. In the case where this perturbation is strong, is there a mechanism that can restore the polarization states of emitted harmonics?

Results obtained for the individual nanoflakes and compound system comprising several identical nanoflakes reveal that selection rules for the circular polarization states of harmonic generation from 10^4 carbon atoms size plasmonic graphene nanoflakes are determined by the microscopic arrangement of carbon atoms.

The peculiarity of the compound system comprising several identical nanoflakes is that its microscopic symmetry might be different (lower) than the microscopic symmetry of individual constituents. In this situation, for the well separated and weakly interacting nanoflakes the generation and polarization of emitted harmonics is driven by their individual microscopic symmetries. Reducing the separation between nanoflakes leads to the emergence of the circularly polarized harmonics specific to the microscopic symmetry of compound system. Therefore, varying the interaction strength allows to control the intensity of the SAM$= \pm 1$ polarisation states at specific harmonic frequencies.

As a direct consequence of the role of the microscopic symmetry determining selection rules for the circular polarisation at harmonic frequencies, a break of this symmetry by e.g. constrained relaxation of graphene lattice because of the substrate, geometry imperfections in the fabrication process, defects and adatoms, potentially might have strong effect on the nonlinear response.

With an example of carbon atom vacancy defects at extremely low concentration, and with an example of the slight misalignment of the one of the nanoflakes in a compound system, we have demonstrated that this is indeed the case. Even slight alternation of the atomic-scale symmetry has strong impact on the nonlinear response. Most important, the circular polarization of the harmonics specific to an ideal nanostructure is lost and it is replaced by the one determined by the C1 symmetry.

Along with revealing the role of breaking the microscopic symmetry, we have analysed possibility to restore the sought circular polarization of the harmonics allowed by selection

rules for an ideal nanostructure. In particular, we have shown that using a large set of noninteracting coherently illuminated defective nanoflakes allows to average out the effect of the symmetry imperfections and to retrieve polarization state of the harmonics specific for the structure without defects.

The main qualitative findings of this study are robust consequence of the symmetry and hold for large variety of graphene nanoflakes considered here. We believe that our results will contribute to the understanding of the general symmetry constraints controlling the polarisation of harmonics emitted by graphene nanoflakes at plasmon resonance with fundamental wave. Moreover, if the behavior of the network of independent nanoparticles as considered here is generalizable to an interacting system, this opens a possibility for design of the high-performance symmetry-selective nonlinear metamaterials, exploiting high and tunable non-linearity of graphene.

Supporting Information Available

The following files are available free of charge. Supporting Information providing

- Derivation of the selection rules for the multipoles of the induced nonlinear charge density.
- Validation of the perturbative regime for nonlinear response for the fundamental electromagnetic pulse used in this work.
- Illustration of the effect of the centering of graphene lattice inside the global shape with an example of triangular graphene nanoflakes.
- Additional results and discussion completing the information presented in Fig. 5
- Dependence of the plasmon resonance on the size of graphene nanoflakes and on the doping level.

- Effect of the vacancy position on nonlinear response.
- The lattice relaxation and nonlinear response of ideal and defective nanoflakes.

References

(1) Zhang, R.; Zhang, Y.; Dong, Z. C.; Jiang, S.; Zhang, C.; Chen, L. G.; Zhang, L.; Liao, Y.; Aizpurua, J.; Luo, Y.; Yang, J. L.; Hou, J. G. Chemical mapping of a single molecule by plasmon-enhanced Raman scattering. *Nature* **2013**, *498*, 82–86.

(2) Jahng, J.; Fishman, D. A.; Park, S.; Nowak, D. B.; Morrison, W. A.; Wickramasinghe, H. K.; Potma, E. O. Linear and Nonlinear Optical Spectroscopy at the Nanoscale with Photoinduced Force Microscopy. *Accounts of Chemical Research* **2015**, *48*, 2671–2679.

(3) Prince, R. C.; Frontiera, R. R.; Potma, E. O. Stimulated Raman Scattering: From Bulk to Nano. *Chemical Reviews* **2017**, *117*, 5070–5094.

(4) Schoetz, J.; Wang, Z.; Pisanty, E.; Lewenstein, M.; Kling, M. F.; Ciappina, M. F. Perspective on petahertz electronics and attosecond nanoscopy. *ACS Photonics* **2019**, *6*, 3057–3069.

(5) Borsch, M.; Meierhofer, M.; Huber, R.; Kira, M. Lightwave electronics in condensed matter. *Nature Reviews Materials* **2023**, *8*, 668–687.

(6) Dombi, P.; Pápa, Z.; Vogelsang, J.; Yalunin, S. V.; Sivis, M.; Herink, G.; Schäfer, S.; Groß, P.; Ropers, C.; Lienau, C. Strong-field nano-optics. *Rev. Mod. Phys.* **2020**, *92*, 025003.

(7) Ludwig, M.; Aguirregabiria, G.; Ritzkowsky, F.; Rybka, T.; Marinica, D. C.; Aizpurua, J.; Borisov, A. G.; Leitenstorfer, A.; Brida, D. Sub-femtosecond electron transport in a nanoscale gap. *Nature Physics* **2020**, *16*, 341–345.

(8) Bionta, M. R.; Ritzkowsky, F.; Turchetti, M.; Yang, Y.; Cattozzo Mor, D.; Putnam, W. P.; Kärtner, F. X.; Berggren, K. K.; Keathley, P. D. On-chip sampling of optical fields with attosecond resolution. *Nature Photonics* **2021**, *15*, 456–4560.

(9) Schlecht, M. T.; Knorr, M.; Schmid, C. P.; Malzer, S.; Huber, R.; Weber, H. B. Light-field-driven electronics in the mid-infrared regime: Schottky rectification. *Science Advances* **2022**, *8*, eabj5014.

(10) Abb, M.; Albella, P.; Aizpurua, J.; Muskens, O. L. All-Optical Control of a Single Plasmonic Nanoantenna–ITO Hybrid. *Nano Letters* **2011**, *11*, 2457–2463.

(11) Krasavin, A. V.; Randhawa, S.; Bouillard, J.-S.; Renger, J.; Quidant, R.; Zayats, A. V. Optically-programmable nonlinear photonic component for dielectric-loaded plasmonic circuitry. *Opt. Express* **2011**, *19*, 25222–25229.

(12) MacDonald, K. F.; Sámson, Z. L.; Stockman, M. I.; Zheludev, N. I. Ultrafast active plasmonics. *Nature Photonics* **2009**, *3*, 55–58.

(13) Butet, J.; Martin, O. J. F. Nonlinear Plasmonic Nanorulers. *ACS Nano* **2014**, *8*, 4931–4939.

(14) Mesch, M.; Metzger, B.; Hentschel, M.; Giessen, H. Nonlinear Plasmonic Sensing. *Nano Letters* **2016**, *16*, 3155–3159.

(15) Cox, J. D.; García de Abajo, F. J. Nonlinear Graphene Nanoplasmonics. *Accounts of Chemical Research* **2019**, *52*, 2536–2547.

(16) Kern, J.; Großmann, S.; Tarakina, N. V.; Häckel, T.; Emmerling, M.; Kamp, M.; Huang, J.-S.; Biagioni, P.; Prangsma, J. C.; Hecht, B. Atomic-Scale Confinement of Resonant Optical Fields. *Nano Letters* **2012**, *12*, 5504–5509.

(17) Wu, T.; Yan, W.; Lalanne, P. Bright Plasmons with Cubic Nanometer Mode Volumes through Mode Hybridization. *ACS Photonics* **2021**, *8*, 307–314.

(18) Schuller, J. A.; Barnard, E. S.; Cai, W.; Jun, Y. C.; White, J. S.; Brongersma, M. L. Plasmonics for extreme light concentration and manipulation. *Nat. Mater.* **2010**, *1*, 193–204.

(19) Stockman, M. I. Nanoplasmonics: past, present, and glimpse into future. *Opt. Express* **2011**, *19*, 22029–22106.

(20) Stoll, T.; Maioli, P.; Crut, A.; Del Fatti, N.; Vallée, F. Advances in femto-nano-optics: ultrafast nonlinearity of metal nanoparticles. *The European Physical Journal B* **2014**, *87*, 260.

(21) Raschke, M. B.; Berweger, S.; Atkin, J. M. In *Plasmonics: Theory and Applications*; Shahbazyan, T. V., Stockman, M. I., Eds.; Springer Netherlands: Dordrecht, 2013; pp 237–281.

(22) Lambrecht, B.; Leitner, A.; Aussenegg, F. Femtosecond decay-time measurement of electron-plasma oscillation in nanolithographically designed silver particles. *Applied Physics B* **1997**, *64*, 269–272.

(23) Koya, A. N. et al. Advances in ultrafast plasmonics. *Applied Physics Reviews* **2023**, *10*, 021318.

(24) Kauranen, M.; Zayats, A. V. Nonlinear plasmonics. *Nature Photonics* **2012**, *6*, 737–748.

(25) Bin Hasan, S.; Lederer, F.; Rockstuhl, C. Nonlinear plasmonic antennas. *Materials Today* **2014**, *17*, 478–485.

(26) Panoiu, N. C.; Sha, W. E. I.; Lei, D. Y.; Li, G.-C. Nonlinear optics in plasmonic nanostructures. *Journal of Optics* **2018**, *20*, 083001.

(27) Krasavin, A. V.; Ginzburg, P.; Zayats, A. V. Free-electron Optical Nonlinearities

in Plasmonic Nanostructures: A Review of the Hydrodynamic Description. *Laser & Photonics Reviews* **2018**, *12*, 1700082.

(28) Butet, J.; Brevet, P.-F.; Martin, O. J. F. Optical Second Harmonic Generation in Plasmonic Nanostructures: From Fundamental Principles to Advanced Applications. *ACS Nano* **2015**, *9*, 10545–10562.

(29) Mikhailov, S. A. Theory of the giant plasmon-enhanced second-harmonic generation in graphene and semiconductor two-dimensional electron systems. *Phys. Rev. B* **2011**, *84*, 045432.

(30) Nookala, N.; Lee, J.; Tymchenko, M.; Gomez-Diaz, J. S.; Demmerle, F.; Boehm, G.; Lai, K.; Shvets, G.; Amann, M.-C.; Alu, A.; Belkin, M. Ultrathin gradient nonlinear metasurface with a giant nonlinear response. *Optica* **2016**, *3*, 283–288.

(31) Keren-Zur, S.; Avayu, O.; Michaeli, L.; Ellenbogen, T. Nonlinear Beam Shaping with Plasmonic Metasurfaces. *ACS Photonics* **2016**, *3*, 117–123.

(32) Chen, S.; Li, K.; Deng, J.; Li, G.; Zhang, S. High-Order Nonlinear Spin–Orbit Interaction on Plasmonic Metasurfaces. *Nano Letters* **2020**, *20*, 8549–8555.

(33) Chen, S.; Li, K.; Deng, J.; Li, G.; Zhang, S. High-Order Nonlinear Spin–Orbit Interaction on Plasmonic Metasurfaces. *Nano Letters* **2020**, *20*, 8549–8555.

(34) Frese, D.; Wei, Q.; Wang, Y.; Cinchetti, M.; Huang, L.; Zentgraf, T. Nonlinear Bicolor Holography Using Plasmonic Metasurfaces. *ACS Photonics* **2021**, *8*, 1013–1019.

(35) Buono, W. T.; Forbes, A. Nonlinear optics with structured light. *Opto-Electronic Advances* **2022**, *5*, 210174–1–210174–19.

(36) Koenderink, A. F.; Alù, A.; Polman, A. Nanophotonics: Shrinking light-based technology. *Science* **2015**, *348*, 516–521.

(37) Krasnok, A.; Tymchenko, M.; Alù, A. Nonlinear metasurfaces: a paradigm shift in nonlinear optics. *Materials Today* **2018**, *21*, 8–21.

(38) Li, G.; Sartorello, G.; Chen, S.; Nicholls, L. H.; Li, K. F.; Zentgraf, T.; Zhang, S.; Zayats, A. V. Spin and Geometric Phase Control Four-Wave Mixing from Metasurfaces. *Laser & Photonics Reviews* **2018**, *12*, 1800034.

(39) Chen, S.; Li, G.; Zeuner, F.; Wong, W. H.; Pun, E. Y. B.; Zentgraf, T.; Cheah, K. W.; Zhang, S. Symmetry-Selective Third-Harmonic Generation from Plasmonic Metacrystals. *Phys. Rev. Lett.* **2014**, *113*, 033901.

(40) Konishi, K.; Higuchi, T.; Li, J.; Larsson, J.; Ishii, S.; Kuwata-Gonokami, M. Polarization-Controlled Circular Second-Harmonic Generation from Metal Hole Arrays with Threefold Rotational Symmetry. *Phys. Rev. Lett.* **2014**, *112*, 135502.

(41) Konishi, K.; Kan, T.; Kuwata-Gonokami, M. Tunable and nonlinear metamaterials for controlling circular polarization. *Journal of Applied Physics* **2020**, *127*, 230902.

(42) Konishi, K.; Akai, D.; Mita, Y.; Ishida, M.; Yumoto, J.; Kuwata-Gonokami, M. Circularly polarized vacuum ultraviolet coherent light generation using a square lattice photonic crystal nanomembrane. *Optica* **2020**, *7*, 855–863.

(43) Sinha-Roy, R.; Hurst, J.; Manfredi, G.; Hervieux, P.-A. Driving Orbital Magnetism in Metallic Nanoparticles through Circularly Polarized Light: A Real-Time TDDFT Study. *ACS Photonics* **2020**, *7*, 2429–2439.

(44) Yang, X.; Mou, Y.; Zapata, R.; Reynier, B.; Gallas, B.; Mivelle, M. An inverse Faraday effect generated by linearly polarized light through a plasmonic nano-antenna. *Nanophotonics* **2023**, *12*, 687–694.

(45) Quijada, M.; Babaze, A.; Aizpurua, J.; Borisov, A. G. Nonlinear Optical Response of a Plasmonic Nanoantenna to Circularly Polarized Light: Rotation of Multipolar

Charge Density and Near-Field Spin Angular Momentum Inversion. *ACS Photonics* **2023**, *10*, 3963–3975.

(46) Geim, A. K.; Novoselov, K. S. The rise of graphene. *Nature Materials* **2007**, *6*, 183–191.

(47) Basov, D. N.; Fogler, M. M.; García de Abajo, F. J. Polaritons in van der Waals materials. *Science* **2016**, *354*.

(48) Xiao, D.; Liu, G.-B.; Feng, W.; Xu, X.; Yao, W. Coupled Spin and Valley Physics in Monolayers of MoS_2 and Other Group-VI Dichalcogenides. *Phys. Rev. Lett.* **2012**, *108*, 196802.

(49) Gong, S.-H.; Alpeggiani, F.; Sciacca, B.; Garnett, E. C.; Kuipers, L. Nanoscale chiral valley-photon interface through optical spin-orbit coupling. *Science* **2018**, *359*, 443–447.

(50) Kim, D.; Seo, M.-K. Experimental Probing of Canonical Electromagnetic Spin Angular Momentum Distribution via Valley-Polarized Photoluminescence. *Phys. Rev. Lett.* **2021**, *127*, 223601.

(51) Jablan, M.; Buljan, H.; Soljačić, M. Plasmonics in graphene at infrared frequencies. *Phys. Rev. B* **2009**, *80*, 245435.

(52) Castro Neto, A. H.; Guinea, F.; Peres, N. M. R.; Novoselov, K. S.; Geim, A. K. The electronic properties of graphene. *Rev. Mod. Phys.* **2009**, *81*, 109–162.

(53) Grigorenko, A. N.; Polini, M.; Novoselov, K. S. Graphene plasmonics. *Nature Photonics* **2012**, *6*, 749–758.

(54) García de Abajo, F. J. Graphene plasmonics: challenges and opportunities. *ACS Photonics* **2014**, *1*, 135–152.

(55) Cox, J. D.; Marini, A.; García de Abajo, F. J. Plasmon-assisted high-harmonic generation in graphene. *Nature Communications* **2017**, *8*, 14380.

(56) Glazov, M.; Ganichev, S. High frequency electric field induced nonlinear effects in graphene. *Physics Reports* **2014**, *535*, 101–138.

(57) Zhou, R.; Guo, T.; Huang, L.; Ullah, K. Engineering the harmonic generation in graphene. *Materials Today Physics* **2022**, *23*, 100649.

(58) Ullah, K.; Meng, Y.; Shi, Y.; Wang, F. Harmonic generation in low-dimensional materials. *Advanced Optical Materials* **2022**, *10*, 2101860.

(59) Manzoni, M. T.; Silveiro, I.; de Abajo, F. J. G.; Chang, D. E. Second-order quantum nonlinear optical processes in single graphene nanostructures and arrays. *New Journal of Physics* **2015**, *17*, 083031.

(60) Zhang, J.; Zhao, W.; Yu, P.; Yang, G.; Liu, Z. Second harmonic generation in 2D layered materials. *2D Materials* **2020**, *7*, 042002.

(61) Soavi, G. et al. Broadband, electrically tunable third-harmonic generation in graphene. *Nature Nanotechnology* **2018**, *13*, 583–588.

(62) Brun, S. J.; Pedersen, T. G. Intense and tunable second-harmonic generation in biased bilayer graphene. *Phys. Rev. B* **2015**, *91*, 205405.

(63) Zhang, Y.; Huang, D.; Shan, Y.; Jiang, T.; Zhang, Z.; Liu, K.; Shi, L.; Cheng, J.; Sipe, J. E.; Liu, W.-T.; Wu, S. Doping-induced second-harmonic generation in centrosymmetric graphene from quadrupole response. *Phys. Rev. Lett.* **2019**, *122*, 047401.

(64) An, Y. Q.; Nelson, F.; Lee, J. U.; Diebold, A. C. Enhanced optical second-harmonic generation from the current-biased graphene/SiO2/Si(001) structure. *Nano Letters* **2013**, *13*, 2104–2109.

(65) Yoshikawa, N.; Tamaya, T.; Tanaka, K. High-harmonic generation in graphene enhanced by elliptically polarized light excitation. *Science* **2017**, *356*, 736–738.

(66) Boyd, R. W.; Gaeta, A. L.; Giese, E. *Springer Handbook of Atomic, Molecular, and Optical Physics*; Springer, 2008; pp 1097–1110.

(67) Simon, H. J.; Bloembergen, N. Second-Harmonic Light Generation in Crystals with Natural Optical Activity. *Phys. Rev.* **1968**, *171*, 1104–1114.

(68) Tang, C. L.; Rabin, H. Selection Rules for Circularly Polarized Waves in Nonlinear Optics. *Phys. Rev. B* **1971**, *3*, 4025–4034.

(69) Alon, O. E.; Averbukh, V.; Moiseyev, N. Selection Rules for the High Harmonic Generation Spectra. *Phys. Rev. Lett.* **1998**, *80*, 3743–3746.

(70) Žd'ánská, P.; Averbukh, V.; Moiseyev, N. High harmonic generation spectra of aligned benzene in circular polarized laser field. *The Journal of Chemical Physics* **2003**, *118*, 8726–8738.

(71) Thongrattanasiri, S.; Manjavacas, A.; García de Abajo, F. J. Quantum Finite-Size Effects in Graphene Plasmons. *ACS Nano* **2012**, *6*, 1766–1775.

(72) Yannouleas, C.; Vigezzi, E.; Broglia, R. A. Evolution of the optical properties of alkali-metal microclusters towards the bulk: The matrix random-phase-approximation description. *Phys. Rev. B* **1993**, *47*, 9849–9861.

(73) Brey, L.; Fertig, H. A. Elementary electronic excitations in graphene nanoribbons. *Phys. Rev. B* **2007**, *75*, 125434.

(74) Lewandowski, C.; Levitov, L. Intrinsically undamped plasmon modes in narrow electron bands. *Proceedings of the National Academy of Sciences* **2019**, *116*, 20869–20874.

(75) Langer, T.; Baringhaus, J.; Pfnür, H.; Schumacher, H. W.; Tegenkamp, C. Plasmon damping below the Landau regime the role of defects in epitaxial graphene. *New Journal of Physics* **2010**, *12*, 033017.

(76) Yan, H.; Low, T.; Zhu, W.; Wu, Y.; Freitag, M.; Li, X.; Guinea, F.; Avouris, P.; Xia, F. Damping pathways of mid infrared plasmons in graphene nanostructures. *Nature Photonics* **2013**, *7*, 394–399.

(77) Aguillon, F.; Borisov, A. G. Atomic-Scale Defects Might Determine the Second Harmonic Generation from Plasmonic Graphene Nanostructures. *The Journal of Physical Chemistry Letters* **2023**, *14*, 238–244.

(78) Kosik, M.; Müller, M. M.; Słowik, K.; Bryant, G.; Ayuela, A.; Rockstuhl, C.; Pelc, M. Revising quantum optical phenomena in adatoms coupled to graphene nanoantennas. *Nanophotonics* **2022**, *11*, 3281–3298.

(79) Aguillon, F.; Marinica, D. C.; Borisov, A. G. Molecule detection with graphene dimer nanoantennas. *The Journal of Physical Chemistry C* **2020**, *124*, 28210–28219.

(80) Ooi, K. J. A.; Tan, D. T. H. Nonlinear graphene plasmonics. *Proceedings of the Royal Society A: Mathematical, Physical and Engineering Sciences* **2017**, *473*, 20170433.

(81) Baudisch, M.; Marini, A.; Cox, J. D.; Zhu, T.; Silva, F.; Teichmann, S.; Massicotte, M.; Koppens, F.; Levitov, L. S.; García de Abajo, F. J.; Biegert, J. Ultrafast nonlinear optical response of Dirac fermions in graphene. *Nature Communications* **2018**, *9*, 1018.

(82) Li, Q. Z.; Elliott, P.; Dewhurst, J. K.; Sharma, S.; Shallcross, S. Ab initio study of ultrafast charge dynamics in graphene. *Phys. Rev. B* **2021**, *103*, L081102.

(83) Nakagawa, K.; Mao, W.; Sato, S. A.; Ago, H.; Rubio, A.; Kanemitsu, Y.; Hirori, H. Hot electron effect in high-order harmonic generation from graphene driven by elliptically polarized light. *APL Photonics* **2024**, *9*, 076107.

(84) Cox, J. D.; Silveiro, I.; García de Abajo, F. J. Quantum Effects in the Nonlinear Response of Graphene Plasmons. *ACS Nano* **2016**, *10*, 1995–2003.

(85) Lindblad, G. On the generators of quantum dynamical semigroups. *Communications in Mathematical Physics* **1976**, *48*, 119–130.

(86) Gorini, V.; Kossakowski, A.; Sudarshan, E. C. G. Completely positive dynamical semigroups of N-level systems. *Journal of Mathematical Physics* **1976**, *17*, 821–825.

(87) Am-Shallem, M.; Levy, A.; Schaefer, I.; Kosloff, R. Three approaches for representing Lindblad dynamics by a matrix-vector notation. 2015; `https://arxiv.org/abs/1510.08634`.

(88) Kosloff, R. Quantum thermodynamics and open-systems modeling. *The Journal of Chemical Physics* **2019**, *150*, 204105.

(89) Leforestier, C.; Bisseling, R.; Cerjan, C.; Feit, M.; Friesner, R.; Guldberg, A.; Hammerich, A.; Jolicard, G.; Karrlein, W.; Meyer, H.-D.; Lipkin, N.; Roncero, O.; Kosloff, R. A comparison of different propagation schemes for the time dependent Schrödinger equation. *Journal of Computational Physics* **1991**, *94*, 59–80.

(90) Low, T.; Avouris, P. Graphene Plasmonics for Terahertz to Mid-Infrared Applications. *ACS Nano* **2014**, *8*, 1086–1101.

(91) Karimi, F.; Knezevic, I. Plasmons in graphene nanoribbons. *Phys. Rev. B* **2017**, *96*, 125417.

(92) Novko, D. Dopant Induced Plasmon Decay in Graphene. *Nano Letters* **2017**, *17*, 6991–6996.

(93) Ooi, K. J. A.; Cheng, J. L.; Sipe, J. E.; Ang, L. K.; Tan, D. T. H. Ultrafast, broadband, and configurable midinfrared all-optical switching in nonlinear graphene plasmonic waveguides. *APL Photonics* **2016**, *1*, 046101.

(94) Nye, J. F. *Physical Properties of Crystals, Their Representations by Tensors and Matrices*; Oxford University Press, 1985.

(95) Alejo-Molina, A.; Hardhienata, H.; Hingerl, K. Simplified bond-hyperpolarizability model of second harmonic generation, group theory, and Neumann's principle. *J. Opt. Soc. Am. B* **2014**, *31*, 526–533.

(96) Wintterlin, J.; Bocquet, M.-L. Graphene on metal surfaces. *Surface Science* **2009**, *603*, 1841–1852, Special Issue of Surface Science dedicated to Prof. Dr. Dr. h.c. mult. Gerhard Ertl, Nobel-Laureate in Chemistry 2007.

(97) Stauber, T.; Peres, N. M. R.; Guinea, F. Electronic transport in graphene: A semiclassical approach including midgap states. *Phys. Rev. B* **2007**, *76*, 205423.

(98) Das Sarma, S.; Adam, S.; Hwang, E. H.; Rossi, E. Electronic transport in two-dimensional graphene. *Rev. Mod. Phys.* **2011**, *83*, 407–470.

(99) Pereira, V. M.; Guinea, F.; Lopes dos Santos, J. M. B.; Peres, N. M. R.; Castro Neto, A. H. Disorder Induced Localized States in Graphene. *Phys. Rev. Lett.* **2006**, *96*, 036801.

(100) Pereira, V. M.; Lopes dos Santos, J. M. B.; Castro Neto, A. H. Modeling disorder in graphene. *Phys. Rev. B* **2008**, *77*, 115109.

(101) Yuan, S.; De Raedt, H.; Katsnelson, M. I. Modeling electronic structure and transport properties of graphene with resonant scattering centers. *Phys. Rev. B* **2010**, *82*, 115448.

(102) Zobelli, A.; Ivanovskaya, V.; Wagner, P.; Suarez-Martinez, I.; Yaya, A.; Ewels, C. P. A comparative study of density functional and density functional tight binding calculations of defects in graphene. *physica status solidi (b)* **2012**, *249*, 276–282.

(103) Kotakoski, J.; Meyer, J. C.; Kurasch, S.; Santos-Cottin, D.; Kaiser, U.; Krasheninnikov, A. V. Stone-Wales-type transformations in carbon nanostructures driven by electron irradiation. *Phys. Rev. B* **2011**, *83*, 245420.

(104) Banhart, F.; Kotakoski, J.; Krasheninnikov, A. V. Structural Defects in Graphene. *ACS Nano* **2011**, *5*, 26–41.

(105) Aguillon, F.; Marinica, D. C.; Borisov, A. G. Plasmons in graphene nanostructures with point defects and impurities. *The Journal of Physical Chemistry C* **2021**, *125*, 21503–21510.

(106) Aguillon, F.; Marinica, D. C.; Borisov, A. G. Atomic-scale control of plasmon modes in graphene nanoribbons. *Phys. Rev. B* **2022**, *105*, L081401.

TOC Graphic